Product shape change by internal stresses

Groen, M.; Zijlstra, G.; San-Martin, D.; Post, J.; De Hosson, J.T.M.

Published in:
Materials & design

DOI:
10.1016/j.matdes.2018.08.013

Publication date:
2018

Materials and Design 157 (2018) 492–500

Contents lists available at ScienceDirect

Materials and Design

journal homepage: www.elsevier.com/locate/matdes

Product shape change by internal stresses

M. Groen [a], G. Zijlstra [b], D. San-Martin [c], J. Post [a,d], J.Th.M. De Hosson [b,*]

[a] Philips Consumer Lifestyle, Oliemolenstraat 5, 9203 ZN Drachten, the Netherlands
[b] Department of Applied Physics, Materials Innovation Institute and Zernike Institute for Advanced Materials, University of Groningen, Nijenborgh 4, 9747 AG Groningen, the Netherlands
[c] Materalia Research Group, Department of Physical Metallurgy, National Centre for Metallurgical Research (CENIM-CSIC), Avda Gregorio del Amo 8, 28040 Madrid, Spain
[d] Engineering & Technology Groningen, ENTEG, University of Groningen, Nijenborgh 4, 9747 AG Groningen, the Netherlands

HIGHLIGHTS

- The predictability and accuracy of the shape changes in the product design
- Coupling between forming and thermal treatment
- Processing steps of forming and thermal treatment are successfully implemented in the Finite Element computer code.

GRAPHICAL ABSTRACT

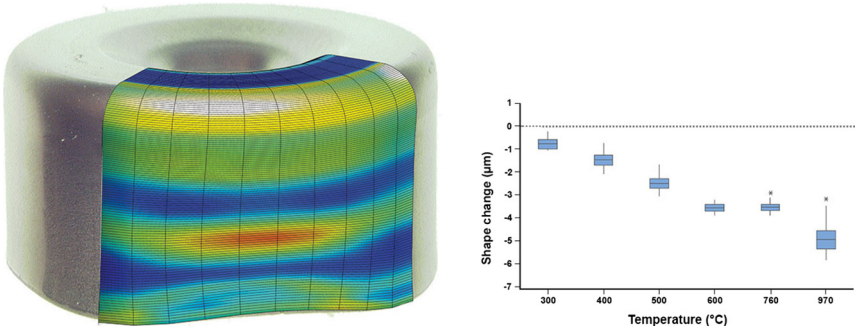

ARTICLE INFO

Article history:
Received 26 May 2018
Received in revised form 26 July 2018
Accepted 5 August 2018
Available online 06 August 2018

Keywords:
Shape change
Residual stress
Phase transformation
Metal forming
Digital twin
FlexMM

ABSTRACT

The design of a product component may require complex processing steps such as metal forming followed by a thermal treatment. The thermal treatment may improve the functional performance of the material itself, but may result in rather unwanted changes in the shape of the product. Here it is shown that Finite Element modeling of the various processes can assist in the design of a robust and accurate production process. The modeling approach presented allows a coupling between various complex material models, in such a way that full cold forming and thermal treatment processes are calculated. This coupling of material models is key for the design and concerns the novelty of the proposed approach. Cold forming by deep drawing is calculated whereby planar anisotropy is implemented. The thermal hardening treatment consists of three contributions: creep, thermal expansion and phase transformation. All models are based on experimental data, acquired from tensile and dilatometer tests, and are implemented into the material model either directly or by a simple fit. It is shown that the effects of a complete forming and heat treatment of a cup could be successfully calculated. The predicted cup shape change was compared to experiments, and shows excellent agreement.

1. Introduction

Miniaturization and net shaping are the trends in manufacturing of consumer products, electronics and automotive, resulting in narrower tolerances for smaller products and more stringent requirements. As a result, the manufacturing process of high precision components suffers from an ever increasing number of complexities, i.e. the components become geometrically more demanding by specifications in three dimensions. Other critical quality requirements such as hardness, surface roughness and density [1–3] have to be produced within narrower specification limits. To keep up with this trend, the development cost of new products as well as the development time of new products have to be reduced. This can be achieved by increasing the predictability

* Corresponding author.
E-mail address: scripta.materialia@rug.nl (J.T.M. De Hosson).

https://doi.org/10.1016/j.matdes.2018.08.013
0264-1275/

of production processes by Finite Element (FE) analysis. The advantage of this numerical analysis is the ability to model complex forming processes. In contrast, the downside of FE analysis is the complexity in preparing input data from experimental results and selection of meaningful output variables.

For the fabrication of high precision metallic parts martensitic high chromium steels are often used. This class of stainless steel is soft in the as-received ferritic phase and therefore a preferred material for complex forming operations. The required hardness is achieved by a thermal hardening treatment, which should not be confused with work hardening. The thermal hardening treatment includes heating up to a temperature of 925 to 1065 °C to transform the ferritic phase into austenite [4], followed by quenching (air cooling is sufficient for this material) to room temperature, to promote the formation of the much harder martensite phase. Although this hardening heat treatment is used to improve the mechanical properties of the cold-formed ferritic product, it comes often at the expense of the shape. If the shape can be maintained and controlled during forming and hardening, the sequential finishing and assembly steps can be a less costly as well as a more energetically efficient process.

Product forming operations as deep drawing, which include stretching and bending, introduce a high residual stress state [5]. Residual stresses arise from the natural shape between different regions, parts or phases [6,7]. These stresses can be measured by destructive techniques such as sectioning, contour, hole-drilling, ring-core and deep-hole [8] through the release of residual stresses upon removal of material from the specimen [9], either on a macroscopic scale or at a local scale [10,11]. Non-destructive methods as X-ray or neutron diffraction [6,12–14], ultrasonic methods and magnetic methods, usually measure a microstructure stress-related parameter [6,9]. The effect of residual stresses on shape changes has been investigated with FE, but focused on individual process steps: during cold forming by finite element modeling [15,16], phase transformation [17] and quenching [18,19].

However, as the individual processes are studied in depth, there is a gap for coupling the dedicated individual models. The aim of this study is to calculate and predict the shape change based on interaction between phenomena rather than presenting a detailed constitutive modeling of the individual material phenomena. The shape change during the thermal treatment calculated with the FEM approach is compared with measurements of the geometry of the real product.

2. Experimental and modeling procedure

The material used in this investigation is a cold rolled strip of the martensitic stainless steel of class AISI 420 with the chemical composition as shown in Table 1.

The studied cup shaped products were fabricated using cold forming, following the design rules and procedures described in [21]. A disk of metal (the blank) is placed in a die with a hole in the middle. The hole is about half the diameter of the disc. The blank is pushed through the hole in the die with a cylindrical punch, causing the sides of the blank to bend over. This bending has to be carefully designed as the material has to be compressed. In this case a tractrix shape (hyperbolic radius) was used for the bending to avoid that the blank has to be pressed flat with a blank holder, and so damaging the ears. The blank is 0.35 mm thick and has a diameter of 32 mm. The resulting cup after this deep drawing has a diameter of 20 mm and a height of about 10 mm. Typically the forming process is followed by a thermal hardening treatment reaching a temperature between 925 and 1065 °C for 30 to 90 min to obtain the desired hardness and strength [4]. The treatment in this work consists of heating with a ramp of 4 °C/s to a temperature of 970 °C. After a dwell time of 900 s, the cups are cooled down to room temperature using a cooling rate 6 °C/s. As it will be described with more details in the following section, the temperature evolution of the yield stress of this material during heating and cooling was experimentally determined using compression (carried out in a plastodilatometer) and tensile tests. The temperature evolution of the relative change in length and the volume fractions of austenite (during heating) and martensite (during cooling) were also obtained using high resolution dilatometry experiments.

Table 1
Chemical composition of AISI 420 class of martensitic stainless steel (wt%) [20].

C	Cr	Si	Mn	P	S	Fe
Min. 0.15	12–14	1	1	0.04	0.030	Bal.

The shape of the cup was recorded at different stages in the process: after forming, during stress relaxation, during annealing and after thermal hardening. The critical geometric parameter for the shape change is the bottom flatness and defined as indicated in Fig. 1. The bottom flatness is defined as the angle between the side of the cup and the top, and measured by scanning the top with a Nanofocus μscan confocal microscope [22]. A radial measurement has been performed at points $r = 9$ mm (y_1) and $r = 7$ mm (y_2). The absolute difference between y_1 and y_2 then quantifies the bottom flatness of the cup. To point out the effect of the thermal cycle on the shape change, the flatness after forming was taken as a reference. The shape change Δ is therefore expressed as $\Delta = (y_1 - y_2)_{forming} - (y_1 - y_2)_{hardening}$. The measured values of y show angular variations caused by the anisotropy in the material. The final value of y is the average over the circumference. To be able to make a statistical comparison and distinguish between reproducible shape defects and distortions, the experiment was repeated for a set of 50 specimens.

Calculation of the cup shape change during forming and the subsequent heat treatment was done using Finite Element Method (FEM). The shape change (or total strain) can be expressed mathematically as the sum of material phenomena; the elastic strain ($\varepsilon_{elastic}$), plastic strain ($\varepsilon_{plastic}$), creep strain (ε_{creep}), thermal strain ($\varepsilon_{thermal}$) and transformation strain ($\varepsilon_{transformation}$):

$$\varepsilon_{tot} = \varepsilon_{elastic} + \varepsilon_{plastic} + \varepsilon_{creep} + \varepsilon_{thermal} + \varepsilon_{transfomation}. \quad (1)$$

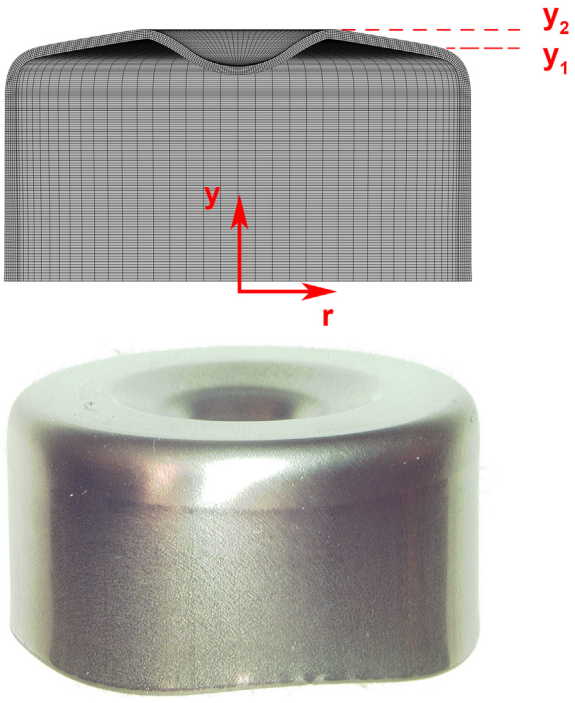

Fig. 1. Real fabricated cup (bottom) and its cross section with points y_1 and y_2. The absolute difference between y_1 and y_2 defines the bottom flatness of the cup.

A regular FEM approach is strongly concentrated on one set of operation at the time, e.g. forming followed by the subsequent heat treatment. When multiple subroutines need to be taken into account simultaneously, the modeling space becomes impractically large as visualized in Fig. 2. Instead, two partial models are preferable. The full process chain model requires a smaller amount of model space. In this work a novel method is used to integrate these two models. The method allows for a model to switch between FE analysis of the forming and the hardening. Since the material model of the forming and the material model of the hardening have a limited physical overlap, the models can be divided with minimal accuracy loss. Filling up the two resulting model spaces with data, results in a lower requirement of measurement data. This approach is called FlexMM, after Flexible Material Model, and is based on previous work [23,24]. The symbols included in the parameter space p (Fig. 2) will be explained in the following sections.

When the material model is split in a metal forming part and a hardening part, it is important to have a thorough understanding of both models and knowledge of which data has to be passed from the forming model to the hardening model. For the new material models, material equations can be used, but also the measurement results can be directly implemented in the FEM parameter space. For the components of Eq. (1):

- The elastic, plastic and creep strains are implemented using the constitutive law;
- The thermal strain, transformation strain and plastic strain at high temperature are experimental data.

The material modeling method to describe a large amount of phenomena at the same time will be explained first. The flow stress of the material is an important material parameter and will be used as an example to express the novel approach. Here, the experimental data can be implemented in the material model, or the constitutive equations can be used. The different contributions to Eq. (1) can be replaced by experimental data, i.e. a measurement graph. In generalized form the flow stress can then be expressed as:

$$\sigma_y = (\varepsilon^p, T, R), \tag{2}$$

with σ_y as the flow stress, ε^p the equivalent plastic strain, R as the anisotropy and T as the temperature. (ε^p, T, Z) represent the state variables of the material model. Based on Eq. (2), the derivative of the flow stress with respect to the state variables can be written as:

$$\dot{\sigma_y} = \frac{\partial \sigma_y}{\partial \varepsilon^p}\dot{\varepsilon}^p + \frac{\partial \sigma_y}{\partial T}\dot{T} + \frac{\partial \sigma_y}{\partial R}\dot{R} \tag{3}$$

The partial derivatives in Eq. (3) are representing the contributions to the general material model of the constitution and can be replaced by a more general formulation:

$$\dot{\sigma_y} = f_{\varepsilon^p}(\varepsilon^p, T, R)\dot{\varepsilon}^p + f_T(\varepsilon^p, T, R)\dot{T} + f_R(\varepsilon^p, T, R)\dot{R} \tag{4}$$

where f_{p_i} represents the derivative of the constitutive model with respect to the parameter space p. Eq. (4) yields:

$$p = [\varepsilon^p, T, R]$$

In a generalized form, p can be stated as:

$$\dot{p}_i = f_{pj}(p)\,\dot{p}_j \text{ here } i \neq j \tag{5}$$

The parameter space p and the functions f_p are the default input for the material modeling routine. In this work a hybrid material model was applied, which uses partly constitutive behavior, and partly experimental data, that was placed directly into the material model.

3. Results

3.1. Cold forming

Calculation of cold forming requires a plasticity model. Due to rolling during manufacturing of the steel, the material is textured. Therefore, the plasticity behavior of the material is not homogeneous for all directions. This anisotropic mechanical behavior of sheet material is described by the Lankford coefficient or planar R-values [25]. The Hill parameters [26] have been calculated from the Lankford parameters using the commercial available software Marc [27] (which will be addressed in the following alinea's).

The R-values are experimentally derived by tensile testing, using the magnitude of the flow stress and the plastic deformation in various directions with respect to the rolling direction. The Hill parameters may vary during the deformation process. Therefore they are implemented

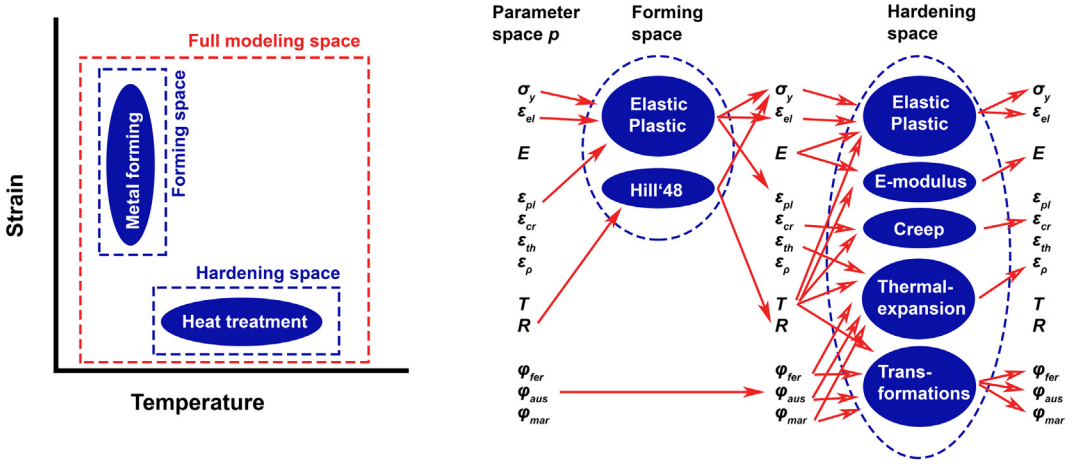

Fig. 2. Schematic of the span of the modeling space for cold forming and heat treatment (Left), and the work flow through the parameter space p and subroutines, in the multi-stage forming-hardening model (Right). The symbols of p represent: σ_y the yield stress, ε_{el} the elastic strain vector, E the elastic modulus, ε_{pl} the equivalent plastic strain, $\varepsilon_{cr}$the equivalent creepstrain, ε_{th} the thermal strain, ε_ρ strain by mass density change, T the temperature, R the anisotropy and φ_{fer}, φ_{aus}, $\varphi_{mar}$the fractions of ferrite, austenite and martensite respectively.

in FEM as a function of the plastic deformation. The function of the Hill parameters therefore becomes:

$$\dot{R} = f_{(1\varepsilon^p)} \quad \varepsilon^p, R_0, R_{90}, R_{45}, \sigma_{0/90}, \sigma_{(0/45)}) \, \dot{\varepsilon}^p, \tag{6}$$

with values of 1.35, 1.81, 1.17, 1.03 and 1.02 for R_0, R_{90}, R_{45}, $\sigma_{0/90}$ and $\sigma_{0/45}$ respectively. The 2D tested planar anisotropic parameters are recalculated to 3D Hill parameters according to [26,27]. R_0 is determined parallel with-, and R_{90} perpendicular to the rolling direction. The evolution of the anisotropy during the metal forming is beyond the scope of this paper, whereupon the function is considered to be constant for this work.

The elastic-plastic behavior is calculated with the FEM software Marc. The subroutine requires a yield curve of the material. The data for the yield curve was acquired by tensile testing and for the higher strains by rolling, and fitted with an Estrin description [28,29]. The flow stress is thus described by a constant *square root of the dislocation density. The resulting flow stress relation for FE implementation becomes:

$$\dot{\sigma}_y = f_{2\varepsilon^p}(\varepsilon^p, R)\dot{\varepsilon}^p. \tag{7}$$

The five coefficients of the original Hill model which define the anisotropy, are encapsulated in parameter *R*. The description of Eq. (7) was used to calculate the cold forming of the cup by deep drawing. The FEM calculation was validated in two ways. First, deep drawing introduces residual stresses. This pre-straining can be related to work–hardening. The calculated stress distribution can be indicated by a hardness measurement profile [30] as was demonstrated in our previous work [29]. Second, the anisotropic behavior is typically exhibited by earing at the open side of the cup. The earing (amplitude and phase) has been calculated and compared to the measured average profiles of 46 cups. The profiles are compared in Fig. 3 and show a good agreement in both the ear-height, as in the phase with respect to the rolling direction. The values of y after forming are 27 μm with a standard deviation of 10 μm.

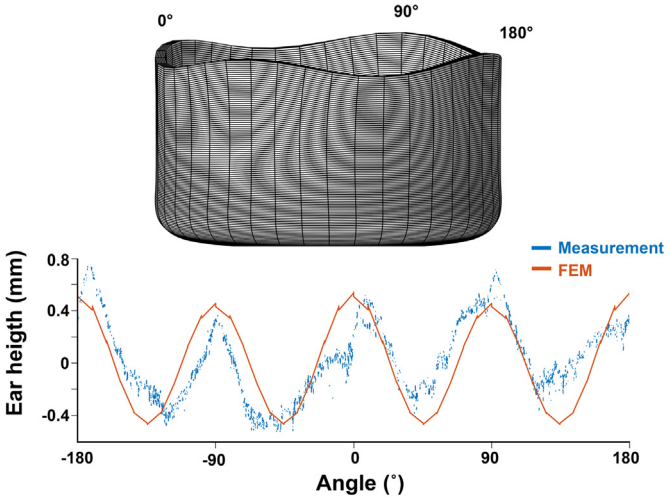

Fig. 3. Result of the metal forming. Top: shape after forming in the FE model. Bottom, comparison of the height of the ears from the calculated cup (solid red line) and a measured specimen (scattered blue dots). The ear profiles vary from cup to cup due to small imperfections like cutting burrs in the blank, which cause large defects in the edge of the cup, but have minor impact on the deep drawing process. Compression at the edge of the cup has a leveraging effect on the edge defects. Also slight eccentric movement during the forming process can affect the height of the individual ears. The specimen showed here suffered less from the possible forming defects, but some imperfections in the blank can still be seen. (For interpretation of the references to colour in this figure legend, the reader is referred to the web version of this article.)

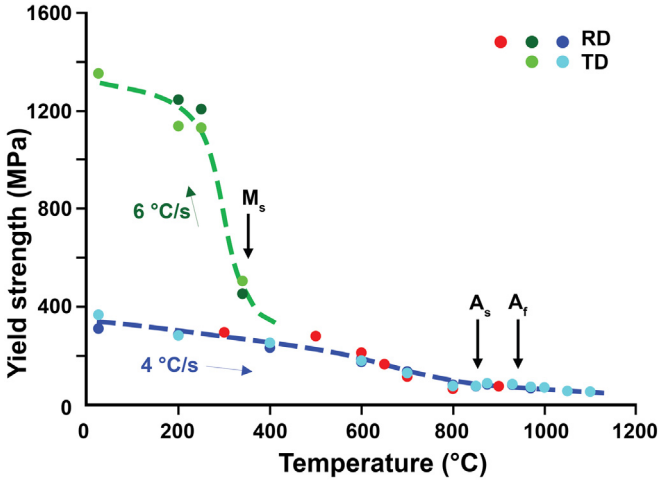

Fig. 4. Temperature evolution of the yield stress during heating up to 1100 °C and cooling down to room temperature. Red full dots have been acquired from tensile tests, while the green and blue full dots correspond to compression tests performed in a plastodilatometer. Symbols RD and TD stand for the rolling and transversal directions. Symbols A_s and A_f stand for the start and end of the ferrite to austenite transformation during heating, while M_s stands for the start of the austenite to martensite phase transformation during cooling. The dashed lines have been drawn as a guide to the eye. (For interpretation of the references to colour in this figure legend, the reader is referred to the web version of this article.)

3.2. Thermal hardening

As it has been described before, the thermal hardening required heating the sample to transform the ferrite into austenite, followed by air cooling to form a martensitic microstructure at room temperature. In Fig. 4 the temperature evolution of the yield stress during the heating and cooling stage is provided Blue and green full dots were determined from compression experiments carried out at 0.01 s^{-1} in a Bähr DIL 805A/D plastodilatometer [31]. For these experiments small cylindrical samples of 5 mm in length and 3 mm in diameter machined along the rolling (RD) and transversal (TD) directions were heated at a rate of 4 °C/s to the testing temperature. A range of temperatures between 25 °C and 1100 °C was tested during heating (light and dark blue full dots). The green full dots corresponds to experiments in which samples, with the same geometry, were heated at 4 °C/s to 970 °C, held for 10 min and cooled at a rate of 6 °C/s to the targeted testing temperature. The red full dots represent the yield stress obtained from tensile test data also during heating up, using a strain rate of 0.012 s^{-1} on samples machined along the rolling direction For these tensile tests, bars of length 430 mm and width 20 mm where cut from a steel plate of 0.5 mm thickness. Indicated by arrows are the austenite start temperature A_S at 852 °C, the austenite finishing temperature A_F at 937 °C and the martensite start temperature M_S at 367 °C. This figure shows that during heating the yield stress decreases continuously down to the range of temperatures where the austenite forms. During cooling, once the M_s has been attained, the hard martensite phase which is now present in the microstructure, increases the yield stress of the steel abruptly, reaching a value of about ~1350 MPa at room temperature (TD sample), compared to yield stress obtained for the initial ferritic microstructure (~370 MPa for the TD sample). There is not a significant dispersion among the results obtained: i) using samples machined along the RD or TD; ii) using tensile or compression samples. Therefore the anisotropy is disregarded for the thermal cycle.

The experimental data is directly implemented in FE. While doing so, one has to distinguish between the heating up and cooling down phase, as the yield stress can have different values for the same temperature depending on the history and phase. The implementation of the

measurements of Fig. 4 in the FE model is therefore split into a description for heating up, and one for cooling down which is valid once the temperature has exceeded the austenite start temperature:

$$\dot{\sigma_y} = f_{3\varepsilon^p}(\varepsilon^p, T)\dot{\varepsilon^p} + f_{1T}(\varepsilon^p, T)\dot{T} \quad if \quad T<A_S \tag{8}$$

$$\dot{\sigma_y} = f_{1T}(T, \varphi_{aus}, \varphi_{mar})\dot{T} + f_{1\varphi_{aus}}(T, \varphi_{aus}, \varphi_{mar})\dot{\varphi}_{aus} + f_{1\varphi_{mar}}(T, \varphi_{aus}, \varphi_{mar})\dot{\varphi}_{mar} \quad if \; T>A_S \tag{9}$$

The fractions of ferrite, austenite and martensite are denoted as φ_{fer}, φ_{aus} and φ_{mar} respectively. It must be noted that the starting microstructure does not only contain ferrite, but also a significant amount of $M_{23}C_6$ carbides that will (partially) dissolve during the formation of austenite. The influence of these carbides on the shape changes has been considered indirectly as it influences the temperature evolution of the yield stress of ferrite, austenite and martensite (Fig. 4), the temperature evolution of the volume fraction of austenite/martensite (Fig. 5) and the relative change in length during heating and cooling (Fig. 6). As the models included in the manuscript rely directly on these experimental results, the influence of carbides has been included.

The stress relaxation during heating of the material is attributed to creep. For an extensive description the reader is referred to [29]. The creep behavior is stress and temperature dependent and leads to the material relation stated in Eq. (10).

$$\dot{\varepsilon}_{creep} = A\left(\frac{b}{d}\right)^{p_{grain}}\left(\frac{\sigma - \sigma_0}{E(T)}\right)^n e^{\frac{-Q_c(T)}{RT}}, \text{ or generalized as } \dot{\varepsilon}_{creep} = f_{1t}(T, \sigma) \tag{10}$$

where b represents the magnitude of the Burgers vector, d is the grain size diameter, p_{grain} represents the grain size exponent. Q_c represents the activation energy for self-diffusion, in bulk or along grain-boundaries or along dislocation cores, depending on the actual operating mechanism. The external applied stress is σ and the threshold stress is σ_0. Young's modulus E is temperature dependent [32–37], and implemented as:

$$\dot{E} = f_{2T}(T)\dot{T} \tag{11}$$

Regarding shape change, phase transformations can be seen best by a change in mass density and thus volumetric change. A mass density of 7.740 kg/m^3 for austenite, and 8.03 kg/m^3 for ferrite and martensite is used. It must be noted that a change in mass density is caused by the thermal expansion and the change in phases, which in this case is ferrite to austenite and austenite to martensite:

$$\dot{\rho} = f_{2\varphi_{aus}}(\varphi_{aus})\dot{\varphi}_{aus} \tag{12}$$

Fig. 5 shows the ferrite to austenite (for different heating rates), and the austenite to martensite transformations derived from high resolution dilatometry experiments. These experiments were carried out on planar samples, 12 mm in length, 4 mm in width and 0.7 mm in thickness using an Adamel Lhomargy DT1000 high resolution dilatometer [38].

The curves cannot be implemented into the material model directly, since the thermal expansion is also incorporated in the results. More

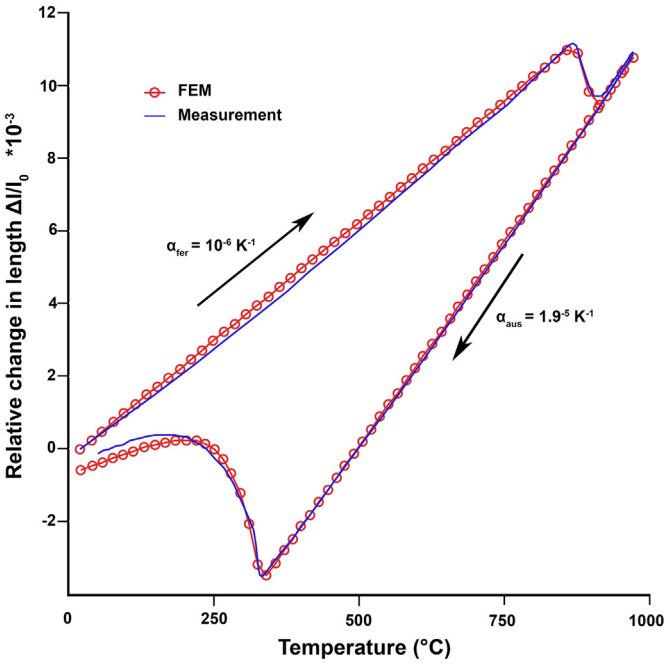

Fig. 6. Temperature evolution of the relative change in length during heating at 4 °C/s up to 970 °C (10 min holding) and subsequent cooling at 6 °C/s. The dark blue solid line corresponds to the experimental behavior recorded by dilatometry, and the red circles reproduce the FE model. (For interpretation of the references to colour in this figure legend, the reader is referred to the web version of this article.)

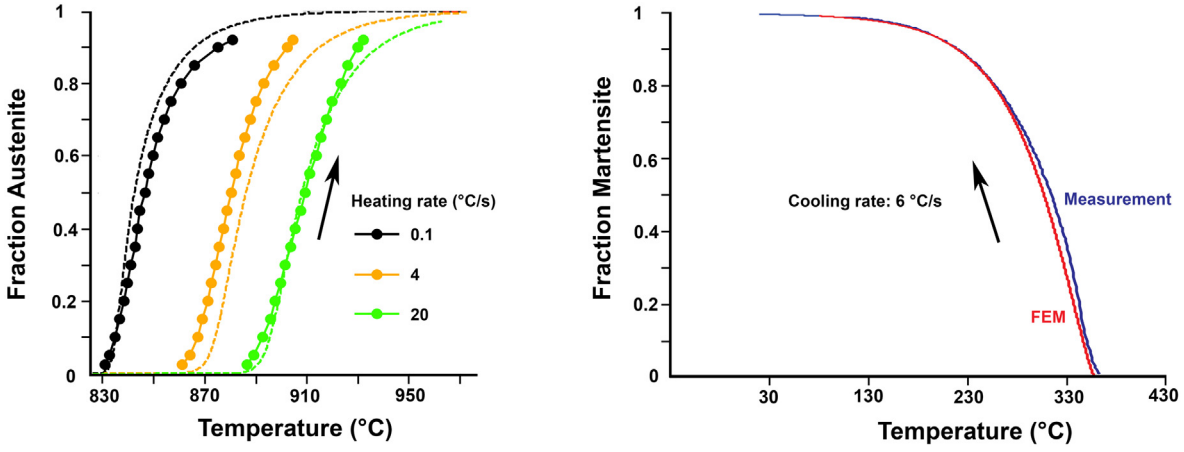

Fig. 5. Temperature evolution of the volume fraction of ferrite to austenite (left plot) and austenite to martensite (right plot) phase transformations during heating and cooling, respectively, as derived from dilatometer tests. Full dots (left plot) correspond to experimental values, while the dashed lines represent the FE model The dark blue solid line (right plot) has been measured experimentally while the red solid line refers to the FE model. (For interpretation of the references to colour in this figure legend, the reader is referred to the web version of this article.)

importantly, as the ferrite to austenite (left plot, Fig. 5) is a diffusional transformation, the heating rate affects atom diffusion involved in the transformation. As the heating rate is increased, the transformation needs higher temperatures to activate the diffusion of the carbon atoms and the transformation shifts to higher temperatures as shown in these figure. Besides, the speed of the transformation might be also influenced by the heating rate. Therefore, a transformation rate description has to be used for this transformation. A (mathematical) Avrami equation [39,40] is used to describe the fraction of a new phase. Starink and Zahra derived an isothermal phase change equation [41,42] in order to obtain a time dependent description. A simple empirical relation is used to integrate start and stop temperatures in this modified JMAK (Johnson-Mehl-Avrami-Kolmogorov) equation: the martensitic transformation (right plot, Fig. 5) as described by Koistinen and Marburger [43]. The main intention of this work is to fit the experimental determined material behavior, in order to demonstrate the capability of this work flow for modeling on a product-sized level.

The relation proposed by Koistinen and Marburger is only temperature dependent and can only facilitate a dual phase transformation. However for the thermal treatment applied here, three phases can be present: ferrite, martensite and austenite.

In reality the dissolution of the carbides causes the inability to transform back into ferrite when the material is in the austenitic phase, but since the carbide evolution was not included in the model, a more practical way to induce the martensitic transformation was applied. In order to avoid that in the calculation the material would transform back into ferrite instead of martensite, the curve is implemented with respect to temperature and phase. A phenomenological relation as shown in Eq. (13) was used to describe the preferred phase in the material. A similar expression is used for the transformation from austenite to martensite.

$$\begin{aligned} \dot{\varphi}_{aus} &= f_{2t}(T) \quad if \quad \varphi_{fer} > 0 \\ \dot{\varphi}_{mar} &= f_{3t}(T) \quad if \quad \varphi_{fer} = 0 \end{aligned} \tag{13}$$

To assure that the material phase transformation is considered in the model in the right order, i.e. from ferrite to austenite and from austenite to martensite, Eqs. (14)–(16) are included in the FE model for the transformation:

$$\dot{\varphi}_{aus} = f_{2t}\left(T, \varphi_{fer}\right) \tag{14}$$

$$\dot{\varphi}_{fer} = f_{3\varphi_{aus}}\left(\varphi_{fer}\right)\dot{\varphi}_{aus} \tag{15}$$

$$\dot{\varphi}_{mar} = f_{4\varphi_{aus}}\left(\varphi_{fer}\right)\dot{\varphi}_{aus} \tag{16}$$

The thermal expansion coefficient has been determined by dilatometry from the temperature dependent evolution of the relative change in length ($\Delta l/l_0$), as shown in Fig. 6. As for Fig. 5, these experiments have been carried out on planar samples, 12 mm in length, 4 mm in width and 0.7 mm in thickness using an Adamel Lhomargy DT1000 high resolution dilatometer. The heating and cooling rates have been 4 and 6 °C/s respectively.

The austenitization conditions used have been 970 °C with a holding time of 10 min. During heating the sample expands linearly up to a temperature (A_s) where the ferrite starts transforming to austenite and the samples contracts; when the transformation has finished (A_f), the sample continues expanding linearly again. During cooling, the sample contracts linearly down to a temperature (M_s) where it starts transforming to martensite and an expansion is recorded. A linear expansion coefficient of 10^{-6} K^{-1} and 1.9^{-5} K^{-1} has been experimentally measured for ferrite and austenite phases respectively. The thermal expansion of martensite is difficult to derive from Fig. 6, and therefore assumed being equal to the thermal expansion of ferrite. The implementation of the thermal expansion coefficient is shown in Eq. (17).

$$\dot{\alpha}_{th} = f_{5\varphi_{aus}}(\varphi_{aus})\dot{\varphi}_{aus} \tag{17}$$

A summary of all the implementations of the thermal hardening model according to Eq. (5), is shown below.

$$\begin{vmatrix} \dot{\sigma}^y \\ E \\ \rho \\ \alpha_{th} \\ \varepsilon^{cr} \\ \varphi_{aus} \\ \varphi_{fer} \\ \varphi_{mar} \end{vmatrix} = \begin{vmatrix} f_{3\varepsilon^p} & f_{1T} & f_{1\varphi_{aus}} & f_{\varphi_{mar}} & 0 \\ 0 & f_{2T} & 0 & 0 & 0 \\ 0 & 0 & f_{2\varphi_{aus}} & 0 & 0 \\ 0 & 0 & f_{5\varphi_{aus}} & 0 & 0 \\ 0 & 0 & 0 & 0 & f_{1t} \\ 0 & 0 & 0 & 0 & f_{2t} \\ 0 & 0 & f_{3\varphi_{aus}} & 0 & 0 \\ 0 & 0 & f_{4\varphi_{aus}} & 0 & 0 \end{vmatrix} \begin{vmatrix} \varepsilon^p \\ T \\ \varphi_{aus} \\ \varphi_{mar} \\ t \end{vmatrix}$$

3.3. Shape change by experiment and FEM predictions

Considerations in the FE model are that the model for anisotropy dictates that the product has symmetry in the 0 and 90 degree direction. Therefore only a quarter of the cup was modeled. This makes it easier to constrain the calculation and speeds up the calculation time considerably. Because of the symmetry the temperature gradient has to be applied in the height direction. The amount of elements over the thickness is very important, as the stress gradients can be large due to deep drawing. To avoid convergence problems and maintain a reasonable calculation time, some boundaries have been set on the calculation as summarized in Table 2. The heat treatment is divided in 4 zones, each calculated in 50 increments: 1) up to 800 °C where creep causes the major deformations. 2) up to 1000 °C where transformation is predominating. 3) Holding (dwelling) with little change, and 4) cooling to room temperature where transformation is the biggest effect. Some increment criteria are set to avoid large change, and thus computational errors.

The initial calculation of the forming of the cup (see Section 3.1) was subjected to a heat treatment up to 970 °C [4], according to the temperature heat treatment described in Section 2. The various implementations for heating described in the previous section, Eqs. (8)–(17), were used to calculate the strains caused by: cold forming, creep, thermal expansion and phase transformation. These calculated strains are displayed in Fig. 7 for different stages of the thermal treatment: elastic strain after cold forming; thermal strain after heating to 970 °C with a thermal gradient of 1 °C; total creep strain after the full thermal cycle (heating and cooling). From the calculations it is observed that:

- Residual stresses have been relaxed due to creep strains before the austenite start temperature (A_s).
- Thermal strains are relatively small, but not homogeneously spread due to an applied thermal gradient.

The critical parameter used to characterized the shape of the cup, the bottom flatness (as described in Section 2), can be extracted from the calculations as a function of temperature. The results are compared to

Table 2
Input values and boundaries for FE calculations.

Setting	Value
Element type	Hexagonal full 3D with 8 nodes
Elements in thickness of blank	6
Angular element steps blank	10
Radial elements in blank	200
Max. increment change	Max value
Equivalent Cauchy stress	100 MPa
Temperature	1000 °C
Strain	0.05

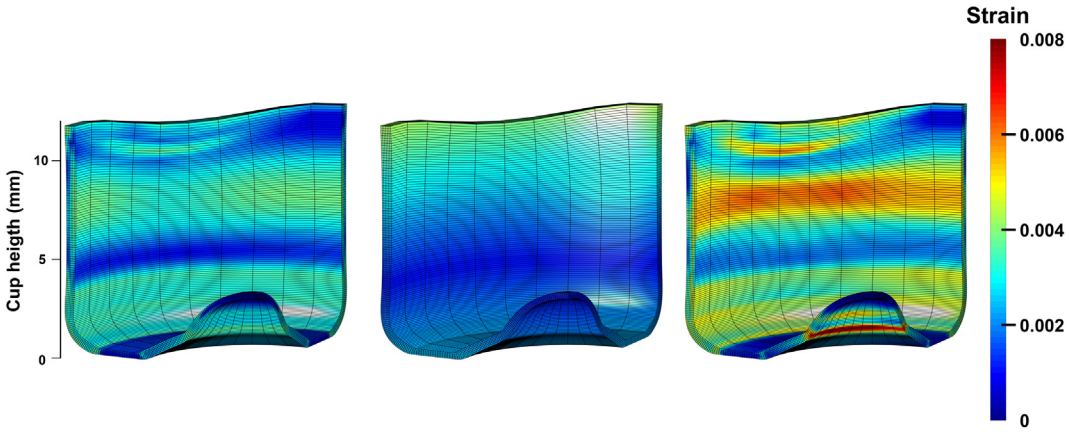

Fig. 7. Example of a FE calculation of the strain distribution in a cold-formed cup at different stages of the thermal treatment. **Left)** elastic strain after cold forming; **Centre)** thermal strain after heating to 970 °C with a thermal gradient of 1 °C; **Right)** total creep strain after the full thermal cycle (heating and cooling).

the experimentally measured shape changes due to the heat treatment (Fig. 8). The shape after forming is taken as the reference values and set to zero (dotted line in Fig. 8). The test samples have to be at room temperature before the shape change can be determined by confocal microscopy. This implies that the samples heated to 970 °C, which is above the austenite start temperature, are actually transformed to martensite during the (air) cooling to room temperature after this temperature has been reached.

The calculations performed with the FEM model have been subjected to the same temperature profile and contain therefore also the austenite to martensite phase transformation. In Fig. 8 can be seen that the bottom flatness decreases as the temperature increases. Up to 300 °C the shape change is the result of plastic deformation due to the decrease of the flow stress with increasing temperature. The majority of the shape change is gained in the following temperature region up to the temperature at which the phase transformation starts (A_s = 852 °C). Here the residual stresses induce the largest strain due to creep processes, which is also seen in Fig. 7. The modeling of the shape change is in good agreement with the experimental values as the same trend is observed in both cases with increasing temperature. The calculations provide a final shape change of 6 μm, and 5.0 ± 0.8 μm for the experimentally measured cups. The shape change of the batches of experimental measured cups is depicted as a box plot [44]

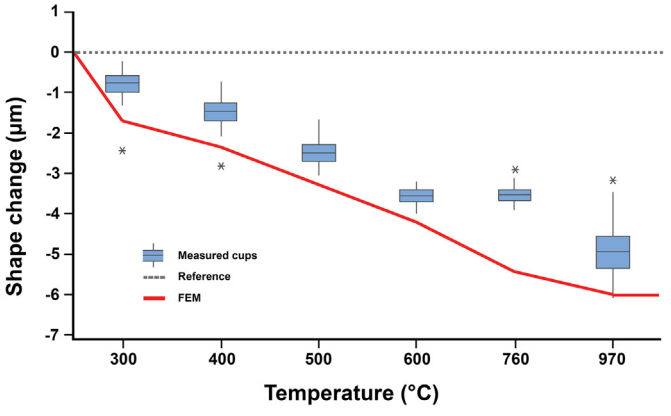

Fig. 8. Cup shape change after heating as predicted by the FEM modeling (solid red line) compared to experimentally measured values (blue box plots). All samples (experimental and calculated) have been cooled down to room temperature before the shape change has been determined. Samples heated to 970 °C have therefore been transformed to martensite. The shape change after forming is taken as a reference value and indicated by the dotted line. The experimental measured values obtained from 46 cups are represented by the box plots. Outliers are indicated by asterisks. (For interpretation of the references to colour in this figure legend, the reader is referred to the web version of this article.)

in order to visualize the spread of the batch values on top of the average value.

4. Discussion

Modeling of the temperature evolution of the cup shape change (Fig. 8) is in general in good agreement with the experimental values. Some deviations compared to the experimental values are observed. Overall the spread for the experimentally measured cups is attributed to small deviations in the forming by deep drawing. A local change of the strain during cold forming could cause a different stress state and stiffness in the product. This can enhance or lessen the occurring shape change during the heat treatment; therefore, the trend of the shape change is more important than the actual values.

The novel contribution of this paper is the successful coupling of a forming and a hardening calculation, in which several material subroutines are called at the same time. Not only has the material behavior been implemented and modeled, but also validated for both the forming and thermal hardening. Thanks to the integrated modeling of both the forming and the hardening, the effect of the metal forming on the shape change after the heat treatment can now be calculated directly. A unique insight in the interactions between the material phenomena and the residual stresses caused by the forming is now created. This model provides the special opportunity to investigate the relative impact of individual parameters, as described in Eqs. (10)–(17), on the cup shape change. The design of the work-flow can be investigated and adjusted, without the necessity of installing a new production setup and performing time consuming experiments. To this end, various parameter changes have been explored, such as:

- amount of material flattening during cold forming;
- the temperature gradient on the product during the heat treatment;
- the heating rate;
- the amount of FEM increments;
- deviation of the experimental determined *E*-modulus;
- deviation of the creep rate.

These calculations are performed in 2D, as opposed to the 3D calculations shown here, to limit the required calculation time. The effect of these parameter changes on the calculated shape change is listed in Table 3. The metal forming shows a strong influence on the calculation. Less flattening results in less shape change after the heat treatment. The flattening of the metal influences the stiffness of the product; more (plastic) deformation can take place when flattening is increased. This alters the residual stress state after forming, which will cause higher creep strains during the thermal treatment [29]. A temperature gradient

Table 3
Effect of adjusted input parameter on the calculated shape change.

Parameter	Adjustment in FEM model	Shape change during heat treatment (%)
Flattening	Lower reduction of material thickness: 30% to 20%	−62.5
Heating rate	Reduced heating rate: 10 °C/s to 1 °C/s	−12.5
Temp. gradient	Reduced temperature gradient: 1 °C to 0 °C	100
Temp. gradient	Increased temperature gradient: 1 °C to 10 °C	300
# of increments	Increase of increments: 200 to 1000	8
E-module	10% lower	8
Creep rate	10% lower	0

can be present in the cup, due to experimental conditions such as furnace design and product throughput. The reference calculation is in good agreement with the experimental results where a temperature gradient of 1 °C is assumed. The calculations with adjusted thermal gradients (none and 10 °C) show a large deviation in shape change and indicate that the thermal gradient is an important parameter in the fabrication process and therefore on the final product quality.

The implementation of the temperature dependent E-modulus, as seen in Eq. (11), assumes a linear temperature dependence up to 800 °C. For temperatures higher than 800 °C no experimental data is available, as the drop in the yield stress and creep effects cause flowing behavior even for low applied stresses. The elastic module is therefore assumed to remain constant above 800 °C. A deviation of E-modulus of 10% seems to have a minor influence on the shape change calculation, as seen in Table 3. Another underlying assumption is that process of relaxation of the residual stresses by creep is faster than the drop of the yield stress due to increasing temperature. The creep rate is also taken as constant from 800 °C up to the phase transformation range of temperatures ($T > A_s$). The influence of this assumption seems not to be of impact on the results, as the calculations with this model show that the residual stresses are already relaxed when a temperature of 700 °C is reached [29]. The calculation with a 10% lower creep rate at every temperature below the transformation one (A_s), does not even show an effect on the calculated cup shape change.

Refinement of the FEM calculation by increasing the amount of steps, has a small influence on the calculated shape change. This indicates that the model is robust with a relatively big time step of 200 increments per load case. This is an important parameter with respect to checking the quality of the FE analysis.

5. Conclusions and outlook

Preliminary investigations of critical parameters indicate that metal forming (flattening) and a temperature gradient have a significant impact on the final cup shape change, and can both positively and negatively influence the product quality. This investigation contributes to the predictability and accuracy of the process chain and shape changes in the product design.

The processing steps of the forming and a thermal treatment have been successfully implemented in the FE code. Cold forming by deep drawing is calculated whereby planar anisotropy is implemented. The important thermal hardening treatment consists of three contributions: creep, thermal expansion and phase transformation. The creep has been predicted using a model developed in [29]. In the present work dilatometer tests have been performed to measure the thermal expansion and phase transformation as a function of temperature and heating rate. Following the new FlexMM approach, the data could be implemented either directly, or after a simple fit, into the material model. With this simplified but robust model, the complete forming and heat treatment of a cup have been successfully calculated. The defined shape change of this cup was compared to experimentally measured shape changes at various temperatures, and showed good agreement.

It has been demonstrated that through modeling a successful coupling between forming and thermal treatment could be made. Measurement and model show that the individual material phenomena can clearly be distinguished in the products during observation as well as the FE model.

Usually the thermal treatment is difficult to adjust in the fabrication process, due to a fixed production setup. Therefore the brief investigation with the FE model is laboriously and costly to validate with a quick series of experiments. However it can be helpful in optimizing the temperature profile and play an important role when a new furnace has to be installed, with a full understanding of the effects of stress and strain during hardening, hereby reducing time and costly experiments.

The metal forming process is more uniform and easier to adjust, however costly due to high investment costs of tooling. With this model the effect of a new tooling design or an adjustment on the current design can now be predicted, but also the interaction with the thermal treatment. This coupling is key in the design of the product discussed in this paper.

Author contribution statement

All authors contributed equally and data is available upon request.

Acknowledgements

This research was carried out under the project number T63.3.12480 in the framework of the research program of the Materials innovation institute M2i, Delft, the Netherlands; and has been part of Press Perfect project, RFSR-CT-2012-00021 funded by the Research Fund for Coal & Steel.

The authors thank Albert Konter, Carola Celada Casero, Mark Veldhuis, Remy Ripandelli, Gerrit Klaseboer, Marijke de Vries, Ronald van der Linden, Daan Waanders, Maarten Oudendijk and Jonas Nilsson, for their important attributions to this work.

References

[1] R. Husson, J.Y. Dantan, C. Baudouin, S. Silvani, T. Schreer, R. Bigot, Evaluation of process causes and influences of residual stress on gear distortion, CIRP Ann. Manuf. Technol. 61 (2012) 551–554, https://doi.org/10.1016/j.cirp.2012.03.106.
[2] C.M. Amey, H. Huang, P.E.J. Rivera-Díaz-del-Castillo, Distortion in 100Cr6 and nanostructured bainite, Mater. Des. 35 (2012) 66–71, https://doi.org/10.1016/j.matdes.2011.10.008.
[3] R. Husson, C. Baudouin, R. Bigot, E. Sura, Consideration of residual stress and geometry during heat treatment to decrease shaft bending, Int. J. Adv. Manuf. Technol. 72 (2014) 1455–1463, https://doi.org/10.1007/s00170-014-5688-8.
[4] ASM International, ASM Handbook Volume 04 - Heat Treating, 1991.
[5] P.J. Withers, Residual stress and its role in failure, Rep. Prog. Phys. 70 (2007) 2211–2264, https://doi.org/10.1088/0034-4885/70/12/R04.
[6] P.J. Withers, H.K.D.H. Bhadeshia, Residual stress. Part 1 – measurement techniques, Mater. Sci. Technol. 17 (2001) 355–365, https://doi.org/10.1179/026708301101509980.
[7] P.J. Withers, H.K.D.H. Bhadeshia, Residual stress. Part 2 – nature and origins, Mater. Sci. Technol. 17 (2001) 366–375, https://doi.org/10.1179/026708301101510087.
[8] D. Peral, C. Correa, M. Diaz, J.A. Porro, J. de Vicente, J.L. Ocaña, Measured strains correction for eccentric holes in the determination of non-uniform residual stresses by the hole drilling strain gauge method, Mater. Des. 132 (2017) 302–313, https://doi.org/10.1016/J.MATDES.2017.06.051.
[9] N.S. Rossini, M. Dassisti, K.Y. Benyounis, A.G. Olabi, Methods of measuring residual stresses in components, Mater. Des. 35 (2012) 572–588, https://doi.org/10.1016/J.MATDES.2011.08.022.
[10] C. Mansilla, D. Martínez-Martínez, V. Ocelík, J.T.M. De Hosson, On the determination of local residual stress gradients by the slit milling method, J. Mater. Sci. 50 (2015) 3646–3655, https://doi.org/10.1007/s10853-015-8927-y.
[11] I. Basu, H. Fidder, V. Ocelík, J. Th.M de Hosson, Local stress states and microstructural damage response associated with deformation twins in hexagonal close packed metals, Crystals 8 (2018) 1–15, https://doi.org/10.3390/cryst8010001.
[12] J. Ahn, E. He, L. Chen, R.C. Wimpory, J.P. Dear, C.M. Davies, Prediction and measurement of residual stresses and distortions in fibre laser welded Ti-6Al-4V considering phase transformation, Mater. Des. 115 (2017) 441–457, https://doi.org/10.1016/J.MATDES.2016.11.078.
[13] K. Hemmesi, M. Farajian, M. Boin, Numerical studies of welding residual stresses in tubular joints and experimental validations by means of x-ray and neutron diffraction analysis, Mater. Des. 126 (2017) 339–350, https://doi.org/10.1016/J.MATDES.2017.03.088.

[14] Z. Wang, E. Denlinger, P. Michaleris, A.D. Stoica, D. Ma, A.M. Beese, Residual stress mapping in Inconel 625 fabricated through additive manufacturing: method for neutron diffraction measurements to validate thermomechanical model predictions, Mater. Des. 113 (2017) 169–177, https://doi.org/10.1016/J.MATDES.2016.10.003.
[15] G. Vastola, G. Zhang, Q.X. Pei, Y.-W. Zhang, Controlling of residual stress in additive manufacturing of Ti6Al4V by finite element modeling, Addit. Manuf. 12 (2016) 231–239, https://doi.org/10.1016/J.ADDMA.2016.05.010.
[16] F. Foadian, A. Carradó, T. Pirling, H. Palkowski, Residual stresses evolution in Cu tubes, cold drawn with tilted dies – neutron diffraction measurements and finite element simulation, Mater. Des. 107 (2016) 163–170, https://doi.org/10.1016/J.MATDES.2016.06.028.
[17] S. Denis, E. Gautier, A. Simon, G. Beck, Stress – phase-transformation interactions – basic principles, modelling, and calculation of internal stresses, Mater. Sci. Technol. 1 (1985) 805–814, https://doi.org/10.1179/026708385790124071.
[18] L. Huiping, Z. Guoqun, N. Shanting, H. Chuanzhen, FEM simulation of quenching process and experimental verification of simulation results, Mater. Sci. Eng. A 453 (2007) 705–714, https://doi.org/10.1016/j.msea.2006.11.023.
[19] C. Simsir, C.H. Gur, 3D FEM simulation of steel quenching and investigation of the effect of asymmetric geometry on residual stress distribution, J. Mater. Process. Technol. 207 (2008) 211–221, https://doi.org/10.1016/j.jmatprotec.2007.12.074.
[20] J.R. Davis, ASM Specialty Handbook: Stainless Steels, 1994.
[21] V.P. Romanovski, Handbook of Cold Stamping, Machinery-Building, Moscow, 1979.
[22] Nanofocus - Mscan Select, http://www.nanofocus.com/products/uscan/uscan-select/ 2015.
[23] J. Post, On the Constitutive Behaviour of Sandvik Nanoflex: Modelling, Experiments and Multi-Stage Forming, http://doc.utwente.nl/50846 2004.
[24] J. Post, M. Groen, G. Klaseboer, Physical model based digital twins in manufacturing processes, Form. Technol. Forum 2017 (2017) 6https://www.researchgate.net/publication/320445237_PHYSICAL_MODEL_BASED_DIGITAL_TWINS_IN_MANUFACTURING_PROCESSES.
[25] W.T. Lankford, S.C. Snyder, J. Bausher, New criteria for predicting the press performance of deep drawing sheets, Trans. Am. Soc. Met. 42 (1950) 1197–1205.
[26] R. Hill, A theory of the yielding and plastic flow of anisotropic metals, Proc. R. Soc. Lond. A. Math. Phys. Sci. 193 (1948) 281–297, https://doi.org/10.1098/rspa.1948.0045.
[27] Marc, Computational Procedures for Elastic-Plastics Analysis, vol. A, 2016 (2016).
[28] Y. Estrin, Dislocation-density–related constitutive modeling, in: A.S. Krausz, K. Krausz (Eds.),Unified Constitutive Laws of Plastic Deformation, 1, 1996, pp. 69–106.
[29] G. Zijlstra, M. Groen, J. Post, V. Ocelík, J.T.M. De Hosson, On the role of the residual stress state in product manufacturing, Mater. Des. 105 (2016) 375–380, https://doi.org/10.1016/j.matdes.2016.05.085.
[30] J. Frankel, A. Abbate, W. Scholz, The effect of residual stresses on hardness measurements, Exp. Mech. 33 (1993) 164–168, https://doi.org/10.1007/BF02322494.
[31] TA Instruments - DIL 805A/D, http://www.tainstruments.com/dil-805ad/ 2013.
[32] J.H. Lee, M. Mahendran, P. Makelainen, Prediction of mechanical properties of light gauge steels at elevated temperatures, J. Constr. Steel Res. 59 (2003) 1517–1532, https://doi.org/10.1016/S0143-974X(03)00087-7.
[33] H.M. Ledbetter, R.P. Reed, Elastic properties of metals and alloys, I. Iron, nickel, and iron-nickel alloys, J. Phys. Chem. Ref. Data 2 (1973) 531–618, https://doi.org/10.1063/1.3253127.
[34] M. Fukuhara, A. Sanpei, Elastic moduli and internal friction of low carbon and stainless steels as a function of temperature, ISIJ Int. 33 (1993) 508–512.
[35] J. Chen, B. Young, Corner properties of cold-formed steel sections at elevated temperatures, Thin-Walled Struct. 44 (2006) 216–223, https://doi.org/10.1016/j.tws.2006.01.004.
[36] J. Chen, B. Young, Experimental investigation of cold-formed steel material at elevated temperatures, Thin-Walled Struct. 45 (2007) 96–110, https://doi.org/10.1016/j.tws.2006.11.003.
[37] H. Masumoto, S. Sawaya, M. Kikuchi, Thermal expansion Young's and temperature modulus in Fe-Cr dependence alloys, Trans. J I M. 12 (1971) 18–21.
[38] C. García de Andrés, F.G. Caballero, C. Capdevila, L.F. Lvarez, Application of dilatometric analysis to the study of solid–solid phase transformations in steels, Mater. Charact. 48 (2002) 101–111https://ac.els-cdn.com/S1044580302002590/1-s2.0-S1044580302002590-main.pdf?_tid=71d0439b-47ce-4bdc-a9cc-197505175407&acdnat=1525781138_8dfca869cced50690cab2ca5312c6238, Accessed date: 8 May 2018.
[39] M. Avrami, Kinetics of phase change. I - general theory, J. Chem. Phys. 7 (1939) 1103, https://doi.org/10.1063/1.1750380.
[40] M. Avrami, Kinetics of phase change. II - transformation-time relations for random distribution of nuclei, J. Chem. Phys. 8 (1940) 212–224, https://doi.org/10.1063/1.1750631.
[41] M.J. Starink, On the meaning of the impingement parameter in kinetic equations for nucleation and growth reactions, J. Mater. Sci. 36 (2001) 4433–4441, https://doi.org/10.1023/A:1017974517877.
[42] M.J. Starink, A.-M. Zahra, An analysis method for nucleation and growth controlled reactions at constant heating rate, Thermochim. Acta 292 (1997) 159–168, https://doi.org/10.1016/S0040-6031(96)03135-8.
[43] D.P. Koistinen, R.E. Marburger, A general equation prescribing the extent of the austenite-martensite transformation in pure iron-carbon alloys and plain carbon steels, Acta Metall. 7 (1959) 59–60.
[44] J.W. Tukey, Exploratory Data Analysis, 1977https://doi.org/10.1007/978-1-4419-7976-6.